Hole Dynamics in Spin and Orbital Ordered Vanadium Perovskites

Sumio Ishihara

Department of Physics, Tohoku University, Sendai 980-8578, Japan

(Received 12 August 2004; published 22 April 2005)

A theory of doped perovskite vanadates with spin and orbital orders is presented. Mobile holes are strongly renormalized by spin excitations (magnons) in the spin G-type and orbital C-type (SG-OC) order, and orbital excitations (orbitons) in the spin C-type and orbital G-type (SC-OG) one. Hole dynamics in a staggered t_{2g} orbital array is distinguished from that in the antiferromagnetic order and the e_g orbital one. The fragile character of the (SG-OC) order in $Y_{1-x}Ca_xVO_3$ is attributed to the orbiton softening induced by a reduction of the spin order parameter.

DOI: 10.1103/PhysRevLett.94.156408 PACS numbers: 71.30.+h, 71.10.−w, 75.30.−m, 78.30.−j

One of the central and as yet not fully understood issues in correlated oxides is the doped Mott insulator and metal-insulator transition (MIT) [1,2]. The prototypical compound is the high T_c superconducting cuprates (HTSC) where holes doped into the antiferromagnetic (AFM) insulating state are strongly renormalized by coupling with spin excitations. There is another class of Mott insulator where the orbital degree of freedom remains. Mobile carriers doped into this class of insulator couple strongly to the orbital array. Perovskite vanadates $R_{1-x}A_xVO_3$ (R = La, Y, A = Ca, Sr) are the likeliest candidate. A number of studies have been done in connection with the spin-orbital orders in RVO_3 [3–12]. In a V^{3+} ion, two electrons occupy the t_{2g} orbitals with the $S = 1$ high-spin state. Two kinds of spin-orbital orders are found in the ground state (see Fig. 1) [3,5]: the G-type (three-dimensional (3D) staggered) spin order (SO) with the C-type (rod type) orbital order (OO) (the alternative $d^1_{xy}d^1_{yz}/d^1_{xy}d^1_{zx}$ configuration) termed (SG-OC) in YVO_3, and the C-type SO with the G-type OO termed (SC-OG) in $LaVO_3$.

Apart from the well studied RVO_3, less is known about the doped Mott insulating $R_{1-x}A_xVO_3$; dynamics of the hole and the spin-orbital background, and their implication for MIT. In the above spin-orbital arrays, the same kinds of orbitals [Fig. 1(a)] or spins [Fig. 1(b)] are aligned along the c axis, in contrast to the staggered spin and orbital order in the ab plane. It is natural to expect that, in the lightly doped region, carriers tend to move along this direction rather than in the ab plane. We are aware that a mobile hole along the c axis is strongly coupled to the spin excitations (magnons) in (SG-OC) [spin-antiferromagnet (AF)] and the orbital ones (orbitons) in (SC-OG) (orbital-AF). Orbiton, standing for a quantized object of the collective orbital excitation, was observed in $LaMnO_3$ [13] and is suggested in RVO_3 [12,5]. Thus, the perovskite vanadates are ideal for study of the quantum hole dynamics controlled by orbiton in comparison with those by magnon. One of the striking differences between the two phases is seen in their stabilities; (SG-OC) is rather fragile against the hole doping [4,14]. This phase in $Y_{1-x}Ca_xVO_3$ rapidly collapses by doping of holes around $x \leq 0.05$, and is changed into (SC-OG) being stable up to $x \sim 0.4$. This anomalously fragile nature of (SG-OC) is hardly explained by the conventional doped 3D AFM with $S = 1$, and suggests the interplay between spin and orbital on the hole dynamics.

Here we present a theory of doped vanadates with spin and orbital orders. Hole dynamics associated with the t_{2g} orbitons is distinguished from that with magnons and the e_g orbitons. The fragile (SG-OC) order is attributed to the strong interplay of spin and orbital on the hole dynamics.

Our starting point is the $t - J$ type model with the t_{2g} orbital degree of freedom, $\mathcal{H} = \mathcal{H}_t + \mathcal{H}_J + \mathcal{H}_{\rm JT}$, derived from the generalized Hubbard model in the large on-site interaction limit [15]. The superexchange term is $\mathcal{H}_J = \mathcal{H}_{^4A_2} + \mathcal{H}_{^2E} + \mathcal{H}_{^2T_1} + \mathcal{H}_{^2T_2}$ where $^4A_2$, ^2E, $^2T_1$, and $^2T_2$ indicate the intermediate $(t_{2g})^3$ configurations. Although all the terms of $\mathcal{H}_J$ are considered in the calculation, here we give explicitly the term with the largest prefactor involving the high-spin $^4A_2$ state as $\mathcal{H}_{^4A_2} = -J_{^4A_2}\frac{1}{6}\sum_{\langle ij\rangle}(2 + \vec{S}_i \cdot \vec{S}_j)h^l_O$ with the $S = 1$ spin operator $\vec{S}_i$, and the exchange interaction $J_{^4A_2}(\equiv J)$ [16]. The complete form of $\mathcal{H}_J$ is presented in Refs. [12,7]. On a given bond along direction $l(= x, y, z)$, the t_{2g} orbitals are classified into two "active" orbitals, a_l and b_l, with a finite electron transfer between the nearest neighboring (NN) sites, and a "inactive" one, c_l, where the transfer is for-

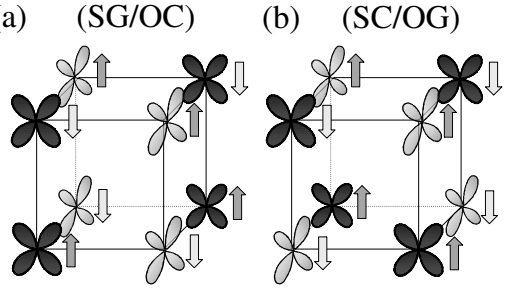

FIG. 1. Schematic spin and orbital structures of (a) (SG-OC) phase and (b) (SC-OG) phase. Commonly occupied d_{xy} orbitals are not shown.

 © 2005 The American Physical Society

bidden. For instance, $(a_z, b_z, c_z) = (yz, zx, xy)$, and for the transfer integral t_γ^l between the NN orbitals γ, we have $t_{yz}^z = t_{zx}^z (\equiv t)$ and $t_{xy}^z = 0$. Then, the orbital part is $h_O^l = -4\vec{\tau}_i^l \cdot \vec{\tau}_j^l + \frac{1}{9}\{4 - \sqrt{2}(v_i^l + v_j^l) - 4v_i^l v_j^l\}$ where we introduce the pseudo-spin operator for the active orbitals $\vec{\tau}_i^l = \frac{1}{2}\sum_{\gamma,\gamma'=(a_l,b_l),\sigma} c_{i\gamma\sigma}^\dagger \vec{\sigma}_{\gamma\gamma'} c_{i\gamma'\sigma}$, and the charge-difference operator between the active and inactive ones $v_i^l = n_{ia_l} + n_{ib_l} - 2n_{ic_l}$. The electron annihilation operator $c_{i\gamma\sigma}$ with spin $\sigma(=\uparrow, \downarrow)$, orbital $\gamma(= yx, zx, xy)$ at site i, the number operator $n_{i\gamma} = \sum_\sigma c_{i\gamma\sigma}^\dagger c_{i\gamma\sigma}$, and the Pauli matrices $\vec{\sigma}$ are also defined. Similar spin-orbital models are derived in Refs. [7–10,17,18]. The Jahn-Teller (JT) coupling is given by $\mathcal{H}_{\rm JT} = g\sum_i \{v_i^z Q_{iEu} + (\vec{\tau}_i^z)_z Q_{iEv}\}$ where $Q_{iEu(v)}$ is the normal modes of an O_6 octahedron with symmetry $E_g u(E_g v)$, which is treated as a classical variable. The (SG-OC) and (SC-OG) orders in $R\mathrm{VO}_3$ are well reproduced by $\mathcal{H}_J + \mathcal{H}_{\rm JT}$ [12]. Apart from the undoped $R\mathrm{VO}_3$, motion of the doped holes is responsible for the t term, $\mathcal{H}_t = \sum_{\langle ij\rangle,\gamma,\sigma}(t_\gamma^l c_{i\gamma\sigma}^\dagger c_{j\gamma\sigma} + \mathrm{H.c.})$.

We turn to the formulation of the hole dynamics in $R_{1-x}A_x\mathrm{VO}_3$. The Schwinger-boson approach associated with the self-consistent Born approximation (SCBA) provides a good description for the lightly doped Mott insulator known in the HTSC [19–22] and the manganites [23]. The hopping of a doped hole in the staggered spin(orbital) alignments induces the "wrong" spin(orbital) configurations, i.e., the magnon(orbiton) excitations. There are two kinds of orbiton modes per V^{3+} ion; excitations of (A) $d_{yz} \leftrightarrow d_{zx}$ and (B) $d_{xy} \leftrightarrow (d_{zx}, d_{yz})$. The type-(B) excitation does not propagate coherently (local mode), because the wrong orbital configurations induced by the hole motion are not recovered by the quantum exchange processes [12]. Besides, the d_{xy} band is separated from the d_{yz}/d_{zx} ones, i.e., the orbiton energy of (B) is higher than that of (A) [6]. Then, we adopt the following expression for the electron operator,

$$c_{i\gamma\sigma} = [\delta_{\gamma=(xy)}\tilde{f}_i \tilde{s}_{i\sigma}^\dagger + \delta_{\gamma=(zx,yz)} f_i s_{i\sigma}^\dagger t_{i\gamma}^\dagger] P_S, \qquad (1)$$

where the type-(A) excitation is only introduced by the bosonic operator $t_{i\gamma}$. The two fermionic operators $\{\tilde{f}_i, f_i\}$ for charge, and the two bosonic ones $\{\tilde{s}_{i\sigma}, s_{i\sigma}\}$ for spin, are introduced with the local constraints [24]. The operator P_S projects onto the ${}^3T_1$ high-spin state in the $(t_{2g})^2$ configuration. In this scheme, the superexchange term $\mathcal{H}_J$ is expressed by the magnon and orbiton operators within the spin-wave approximation [12]. The mean-field type decoupling is introduced in $\mathcal{H}_J$; in the magnon (orbiton) part expressed by $s_{i\sigma}$ ($t_{i\gamma}$), the orbital (spin) operators are replaced by the static correlation function $\langle \tau_i^l \tau_j^l \rangle$ ($\langle \vec{S}_i \cdot \vec{S}_j \rangle$). The quantum spin-orbital coupled dynamics are expected to be suppressed by the JT coupling [9] and the $S = 1$ spin. $\mathcal{H}_J$ is diagonalized by the Bogoliubov transformation.

It is clear that the hole motion in the ab plane is common to both (SG-OC) and (SC-OG), and is not enough to explain the different hole dynamics and stability of the two phases. Similar physical consequences are only to be expected from the d_{xy}-hole motion to those in a mobile $d_{x^2-y^2}$ hole in the 2D quantum AFM, which is studied well in HTSC [19]. The d_{yz}/d_{zx}-hole motion in the ab plane is associated with the simultaneous magnon-orbiton coupled excitations which is supposed to be suppressed as discussed above. Then, we focus on the motion of the d_{yz}/d_{zx} hole along the c axis characterizing different hole dynamics in the two spin-orbital phases. This part of the t term $\mathcal{H}_t$ is

$$\mathcal{H}_{yz/zx}^c = -\frac{4t}{\sqrt{N}}\sum_{\vec{k},\vec{q}} f_{\vec{k}}^\dagger f_{\vec{k}-\vec{q}}\left\{g_{\vec{k}-\vec{q}} u_{\vec{q}} + g_{\vec{k}} u_{-\vec{q}}^\dagger\right\}, \qquad (2)$$

where $u_{\vec{q}} = s_{\vec{q}}$ for (SG-OC) and $u_{\vec{q}} = t_{\vec{q}}$ for (SC-OG) with $g_{\vec{k}} = \cos ak_z$. The mobile hole along the c axis is coupled to magnon (orbiton) in (SG-OC) [(SC-OG)].

The hole dynamics is examined by calculating the electron spectral function $A_{\vec{k}}(\omega)$ for the fermion propagator $G_{\vec{k}}(\omega)$. In SCBA, the self-energy [Fig. 2(a)] is $\Sigma_{\vec{k}}(\omega) = \frac{i}{2\pi N}\int d\nu \sum_{\vec{q}} G_{\vec{k}-\vec{q}}(\omega - \nu)|\Gamma_{\vec{k},\vec{q}}^{(u)}|^2 D_{\vec{q}}^{(u)0}(\nu)$ where $u = s$ for (SG-OC) and $u = t$ for (SC-OG). We introduce the bare boson propagator $D_{\vec{q}}^{(u)0}(\nu)$ and the renormalized-coupling constant $\Gamma_{\vec{k},\vec{q}}^{(u)}$ expressed by $g_{\vec{k}}$ and the coefficients for the Bogoliubov transformation by which $\mathcal{H}_J$ is diagonalized. An infinite class of the noncrossing diagrams is summed up by ignoring the vertex correction [19,20,24]. A reasonable parameter set as $J/t = 0.2$ and $gQ_E/J = 1$–1.25 with J being around 30 meV is chosen [9,12].

In both the two phases, $A_{\vec{k}}(\omega)$ (Fig. 3) shows the broad incoherent continuum and the well-separated quasiparticle (QP) peak. The dispersive QP peak has the band width of the order of J and has the highest energy at the momentum $(0, 0, \frac{\pi}{2a})$ with a being the cubic perovskite lattice constant [25]. Let us focus on $A_{\vec{k}}(\omega)$ in (SC-OG) (orbital-AF); a large portion of the spectra is concentrated on the QP peak, and the QP weight $a_{\vec{k}}$ is rapidly saturated with increasing J (the inset of Fig. 3). This is clearly in contrast to both the

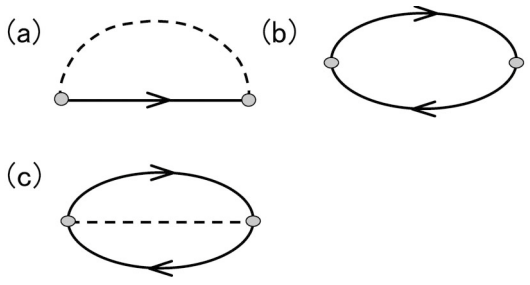

FIG. 2. Diagrams for (a) the self-energy of electron, (b) that of magnon(orbiton), and (c) the optical conductivity. Bold lines are for the full-fermion propagators and broken lines are for the bare-magnon (orbiton) ones in the (SG-OC) [(SC-OG)] phase.

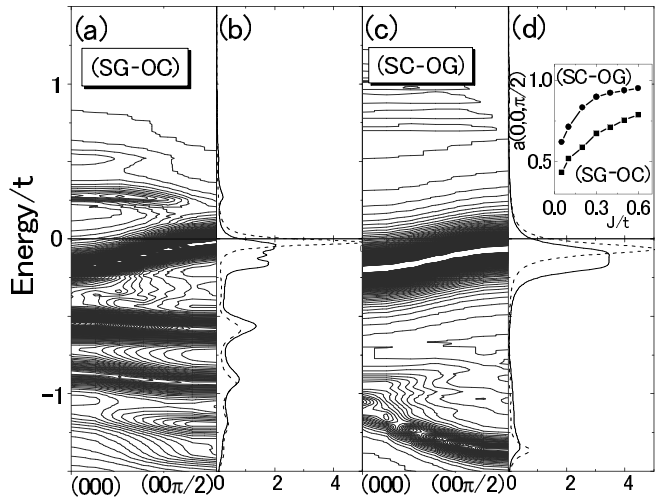

FIG. 3. Contour plot of spectral function and DOS of electrons in (SG-OC) [(a) and (b)], and those in (SC-OG) [(c) and (d)] for $x = 0.1$. Bold lines in (b) and (d) are for DOS and broken lines are for $A_{(0,0,\frac{\pi}{2a})}(\omega)$ multiplied by $1/5$. The origin of the vertical axis indicates the Fermi energy. The inset in (d) shows the QP weight at $\vec{k} = (0, 0, \frac{\pi}{2a})$.

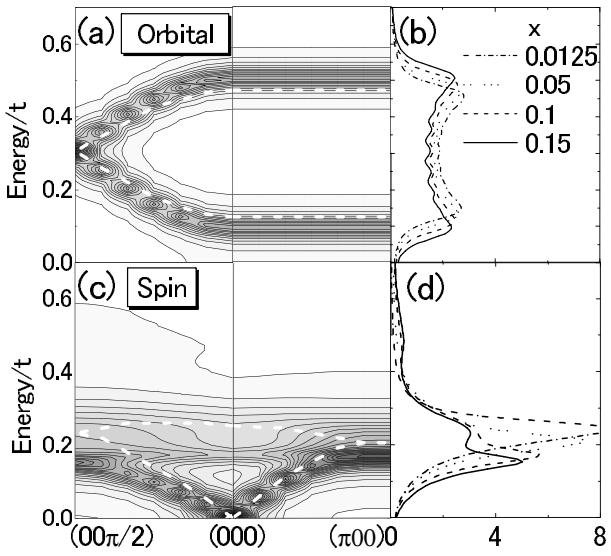

FIG. 4. Contour plots of the spectral functions at $x = 0.1$ and the DOS for orbiton (a) and (b) and those for magnon (c) and (d) in (SG-OC). White broken lines in (a) and (c) indicate dispersion relations at $x = 0$. The lower branch of the orbiton in (a) corresponds to that along $(0, 0, \frac{\pi}{2a}) - (0, 0, \frac{\pi}{a}) - (\frac{\pi}{a}, 0, \frac{\pi}{a})$ in the Brillouin zone for the cubic perovskite unit cell.

case of (SG-OC) (spin AF), where the spectra are widely distributed to the incoherent part, and the ladder-type spectra seen in the $t - J_z$ model [20]. Those characters of $A_{\vec{k}}(\omega)$ in (SC-OG) are ascribed to the large orbiton energy with the gap about $2J$–$3J$ which suppresses the low-energy inelastic scattering of holes, unlike the magnon excitation in (SG-OC). The spectra in (SC-OG) are also distinguished from those in the e_g orbital order studied in doped manganites [23,26]; $A_{\vec{k}}(\omega)$ has a large weight around the free e_g bands with the band width of the order of t, rather than the QP peak. This is because the orbital order parameter is conserved in the present t_{2g} case, in contrast to the e_g case, where the nonzero hopping matrices between the different orbitals break the conservation.

Then we turn to the spin and orbital sectors, especially, in the (SG-OC) phase. The magnon-orbiton propagators are given by the bubble-type self-energy diagram [Fig. 2(b)]; $\Pi^{(u)}_{\vec{q}}(\omega) = \frac{-i}{2\pi N}\int d\nu \sum_{\vec{k}} |\Gamma^{(u)}_{\vec{k},\vec{q}}|^2 G_{\vec{k}+\vec{q}}(\omega+\nu) \times G_{\vec{k}}(\nu)$. The spectral functions $S_{\vec{q}}(\omega)$ for magnon and $T_{\vec{q}}(\omega)$ for orbiton, and their density of states (DOS) in (SG-OC) are shown in Fig. 4. In the undoped case (white broken lines), $S_{\vec{q}}(\omega)$ well reproduces the experimental magnon dispersion in YVO_3 [11]. The flat dispersion of $T_{\vec{q}}(\omega)$ in the ab plane originates from no coherent propagation of the orbiton in this plane [12]. The excitation gap in $T_{\vec{q}}(\omega)$ at $x = 0$ comes from the discontinuous symmetry of the orbital sector in $\mathcal{H}_J$ and the JT interaction, and the gap energy is much smaller than that in (SC-OG) [see Fig. 5(b)]. Namely, the barely stable character of the C-type OO subsists in the undoped state. As expected from distortions of the staggered spin array by mobile holes, softening and broadening are observed in $S_{\vec{q}}(\omega)$ [Figs. 4(c) and 4(d)]. Surprisingly, the bandwidth of $T_{\vec{q}}(\omega)$ becomes broader with doping [Figs. 4(a) and 4(b)], despite that the orbital distortion by hole motion is not caused directly along the c axis. The minimum energy $\omega^{\mathrm{Min}}_{\mathrm{OW}}$ of $T_{\vec{q}}(\omega)$ is located along $\Gamma - X$ in Fig. 4(a) corresponding to $(k_x, k_y, \frac{\pi}{a})$ for the cubic perovskite unit cell. $\omega^{\mathrm{Min}}_{\mathrm{OW}}$ decreases with doping and finally touches the zero energy. That is, the (SG-OC) phase is unstable against the small doping and is changed into the G-type OO where the

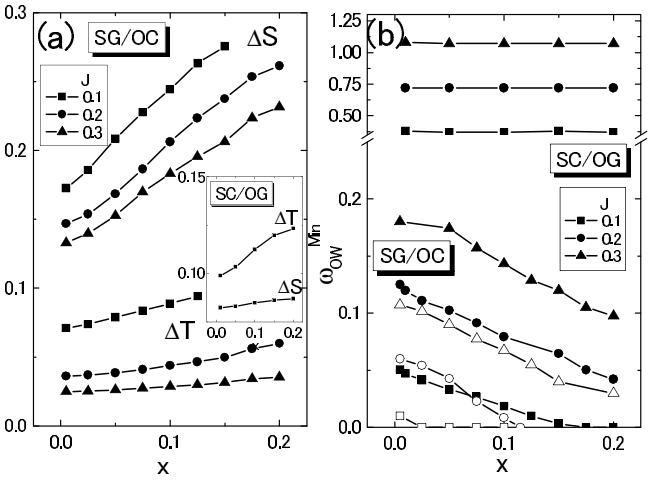

FIG. 5. (a) Reductions of the spin and orbital order parameters, ΔS and ΔT, in (SG-OC). The inset shows those in (SC-OG) with $J/t = 0.2$. (b) The minimum orbiton energy $\omega^{\mathrm{Min}}_{\mathrm{OW}}$. The filled and open symbols in (b) are for $gQ_E/J = 1.25$ and 1, respectively.

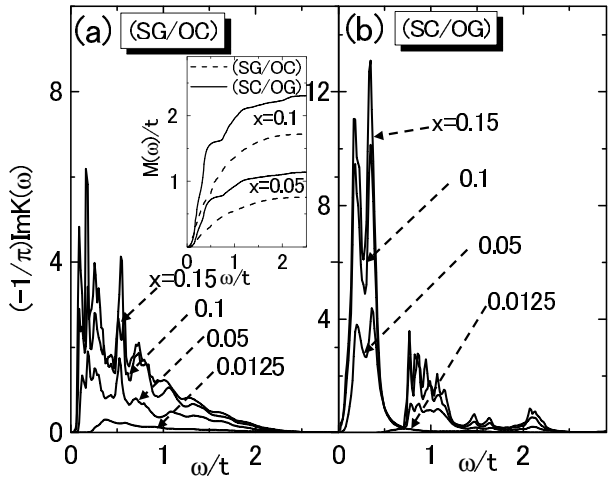

FIG. 6. Regular parts of the optical conductivity spectra for (SG-OC) (a), and those for (SC-OG) (b). The inset in (a) shows the integrated spectral weights for (SG-OC) (broken lines) and those for (SC-OG) (bold lines).

C-type SO is stable. This orbiton softening originates from the reduction of the staggered spin order parameter $\Delta S(\equiv \langle S_{\vec{q}=(\pi\pi 0),(\pi\pi\pi)}\rangle - 1)$ (Fig. 5). The remarkable change by doping is only observed in ΔS of the (SG-OC) phase. However, this reduction itself is not sufficient for instability of the G-type SO, i.e., $\Delta S \ll S(=1)$. Instead, the effective exchange interaction for the staggered (uniform) orbital configuration $J^{\rm orb}_{\rm AF} = J_{4_{A_2}}(2 + \langle \vec{S}_i \cdot \vec{S}_j \rangle)$ [$J^{\rm orb}_{\rm F} = J_{2_{E(^2T_1,^2T_2)}}(1 - \langle \vec{S}_i \cdot \vec{S}_j \rangle)$], increases (decreases) with increasing ΔS. Then, the orbiton energy becomes zero at the critical x. In short, the reduction of the AF spin correlation due to the hole motion softens the orbiton through the spin-orbital interaction, and causes the instability of (SG-OC) to (SC-OG) observed in $Y_{1-x}Ca_xVO_3$ [14].

Finally, we demonstrate that the optical experiment is a good probe to detect directly the qualitatively different hole dynamics. The z component of the optical conductivity spectra is given by $\sigma_{zz}(\omega) = -\frac{(9te)^2}{c^2}{\rm Im}K(\omega)$ with $K(\omega) = \frac{2}{(2\pi N)^2\omega}\int d\omega_1 d\omega_2 \sum_{\vec{k}_1,\vec{k}_2} |\Gamma^{(u)}_{\vec{k}_1,\vec{k}_2}|^2 G_{\vec{k}_1}(\omega_1) \times D^{(u)0}_{\vec{k}_2-\vec{k}_1}(\omega - \omega_1 + \omega_2) G_{\vec{k}_2}(\omega_2)$. This indicates the particle-hole pair creation associated with magnon or orbiton [Fig. 2(c)]. We show the regular part of $\sigma_{zz}(\omega)$ at finite frequency in Fig. 6. With increasing holes, sharp peak structures growing up around $\omega = 0.3J$ and J in (SC-OG), reflecting the large QP weight in $A_{\vec{k}}(\omega)$ (Fig. 3), in contrast to the broad incoherent spectra in (SG-OC). A shoulder structure is clearly seen in the integrated spectral weight $M(\omega) = \frac{c^2}{(9te)^2}\int_0^\omega \sigma_{zz}(\omega')d\omega'$ (the inset of Fig. 6) which would be an evidence characterizing the hole dynamics in the orbital ordered insulators.

In summary, we present a theory of doped vanadium perovskites with spin and t_{2g} orbital orders, beyond the previous theoretical studies on undoped RVO_3. The doped vanadates with the two spin-orbital orders are characterized by the hole motion accompanied by magnon and orbiton. The QP associated with the t_{2g} orbiton is distinguished from that with magnon and the e_g orbiton. The fragile nature of (SG-OC) observed in $Y_{1-x}Ca_xVO_3$ is explained by the strong spin-orbital interplay on the doped hole. These are ascribed to the t_{2g} orbital characters, i.e., the conservation of the orbital order parameter and the finite orbiton gap.

The author would like to thank T. Hatakeyama, S. Maekawa, S. Miyasaka, and Y. Tokura for valuable discussions. This work was supported by KAKENHI from MEXT, KURATA foundation, and CREST. Part of the numerical calculation was performed by the supercomputers in IMR, Tohoku Univ., and ISSP, Univ. of Tokyo.

[1] M. Imada, *et al.*, Rev. Mod. Phys. **70**, 1039 (1998).
[2] S. Maekawa, *et al.*, *Physics of Transition Metal Oxides*, (Springer-Verlag, Berlin, 2004); and references therein.
[3] Y. Ren *et al.*, Phys. Rev. B **62**, 6577 (2000).
[4] S. Miyasaka *et al.*, Phys. Rev. Lett. **85**, 5388 (2000).
[5] S. Miyasaka *et al.*, Phys. Rev. B **68**, 100406 (2003); Phys. Rev. Lett. **94**, 076405 (2005).
[6] H. Sawada *et al.*, Phys. Rev. B **53**, 12 742 (1996).
[7] G. Khaliullin *et al.*, Phys. Rev. Lett. **86**, 3879 (2001).
[8] P. Horsch *et al.*, Phys. Rev. Lett. **91**, 257203 (2003).
[9] Y. Motome *et al.*, Phys. Rev. Lett. **90**, 146602 (2003).
[10] S.-Q. Shen *et al.*, Phys. Rev. Lett. **88**, 027201 (2002).
[11] C. Ulrich *et al.*, Phys. Rev. Lett. **91**, 257202 (2003).
[12] S. Ishihara, Phys. Rev. B **69**, 075118 (2004).
[13] E. Saitoh *et al.*, Nature (London) **410**, 180 (2001).
[14] J. Fujioka, S. Miyasaka, and Y. Tokura, *Meeting Abstracts of the Physical Society of Japan* (Physical Society of Japan, Tokyo, 2004) Vol. 59, Issue 2, p. 448; in YVO_3, (SG-OC) and (SC-OG) are observed in 75 K $< T <$ 120 K and $T <$ 75 K, respectively, (also see Ref. [3]). Around $x = 0.02$ in $Y_{1-x}Ca_xVO_3$, (SC-OG) is changed into (SG-OC) which survives, at least above $x = 0.4$.
[15] S. Ishihara *et al.*, Phys. Rev. B **65**, 064442 (2002).
[16] The exchange interactions in other terms are expressed by $J_{4_{A_2}}$ and a parameter $r_J(\equiv I/U')$ with the on-site inter-orbital Coulomb interaction U' and exchange one I. This value is chosen to be $r_J = 0.125$.
[17] K. I. Kugel *et al.*, Sov. Phys. Solid State **17**, 285 (1975).
[18] A. B. Harris *et al.*, Phys. Rev. Lett. **91**, 087206 (2003).
[19] C. L. Kane *et al.*, Phys. Rev. B **39**, 6880 (1989).
[20] G. Martínez and P. Horsch, Phys. Rev. B **44**, 317 (1991).
[21] J. Igarashi and P. Fulde, Phys. Rev. B **45**, 12 357 (1992).
[22] G. Khaliullin *et al.*, Phys. Rev. B **47**, 463 (1993).
[23] J. van den Brink *et al.*, Phys. Rev. Lett. **85**, 5174 (2000).
[24] The following constraints are imposed: $\tilde{f}^\dagger_i \tilde{f}_i + \sum_\sigma \tilde{s}^\dagger_{i\sigma}\tilde{s}_{i\sigma} = 1$, $f^\dagger_i f_i + \sum_\sigma s^\dagger_{i\sigma} s_{i\sigma} = 1$, and $\sum_\sigma s^\dagger_{i\sigma} s_{i\sigma} = \sum_{\gamma=(yz,zx)} t^\dagger_{i\gamma} t_{i\gamma}$.
[25] S. Ishihara *et al.*, J. Magn. Magn. Mater. **272-276**, 412 (2004).
[26] W. Koshibae *et al.*, Physica C (Amsterdam) **317-318**, 205 (1999).